

Well-balanced scheme for modeling open-channel and surcharged flows in steep-slope closed conduit systems

Arturo S. Leon¹, Christopher Gifford-Miears², and Yunji Choi³

ABSTRACT

The model presented herein is the same as that of Leon et al. (2010b), except that it has been modified to preserve “lake at rest” conditions in sloped prismatic conduits. The results of the new model (present paper) are identical to those of Leon et al. (2010b) for non-rest conditions. These schemes are based on the two-governing equation model, where open channel flows are simulated using the Saint-Venant equations and pressurized flows using the compressible water hammer equations. The new model preserves “lake at rest” conditions (horizontal still water) regardless of the conduit slope, resolves moving jump discontinuities over dry-beds in sloped conduits, and resolves small perturbations from steady-states, even when adjacent to dry regions. The preserving steady-state capability of the new model is of particular importance in continuous long simulations when the conduits are relatively steep ($|S_o| > \sim 0.5\%$). Two main contributions are presented here, namely: (1) a new method for water stage reconstruction that preserves “lake at rest” conditions regardless of the pipe slope, and (2) a horizontal system of coordinates, instead of the commonly used inclined coordinate system, is used for facilitating

¹Assistant Professor, School of Civil and Construction Engineering, Oregon State University, 220 Owen Hall, Corvallis, OR 97331-3212, USA. E-mail: arturo.leon@oregonstate.edu (Corresponding author)

²Graduate Research Assistant, School of Civil and Construction Engineering, Oregon State University, 231 Owen Hall, Corvallis, OR 97331-3212, USA. E-mail: giffordc@onid.orst.edu

³Graduate Research Assistant, School of Civil and Construction Engineering, Oregon State University, 231 Owen Hall, Corvallis, OR 97331-3212, USA. E-mail: choiyun@onid.orst.edu

the implementation of the proposed well-balanced scheme to complex systems. In the horizontal coordinate system, the cross-section of a circular pipe becomes an ellipse. The hydraulic characteristics of an ellipse are presented. Good results are achieved in the test cases.

Keywords: Combined sewer system; Finite volume method; Open-channel flow; Storm-water system, Surcharged flow Transient flow; Unsteady flow, Well-balanced scheme.

INTRODUCTION

The design and operation of storm-water and combined sewer systems often require transient and non-transient analysis of these systems. Usually, transient analysis is of interest in short periods of simulation when the system boundary conditions change rapidly (e.g., gate closing/opening, pump failure), while as non-transient analysis is important in long periods of simulation (e.g., continuous simulation) when the system boundary conditions change slowly. Some simulations may require to combine transient and non-transient analysis, such as in continuous simulations when the interest is on assessing the transient and non-transient system response to a series of storm events.

It has been widely recognized that Finite Volume (FV) methods are well suited for solving hyperbolic systems of equations that permit various discontinuities such as shocks (e.g., LeVeque 2002). Various FV methods have been applied to transient open-channel and surcharged flows (i.e., pressurized flows) in closed conduits (e.g., Capart et al. 1997; Bourdarias and Gerbi 2007; Leon et al. 2009 and 2010b; Sanders and Bradford 2011). However most of these approaches do not address “lake at rest” conditions when the slope of the pipe is relatively large ($|S_o| > \sim 0.5\%$). Preserving “lake at rest” conditions is of particular importance when the system is near or at “lake at rest” conditions for relatively long periods of time. The sloped conduits may be completely or partially submerged. A model that is not designed to preserve “lake at

rest” conditions may lead to “numerical storms” when the flow velocity is at or near zero. Numerical storms may produce non-physical oscillations of the water surface and relatively large flow velocities.

Models that are designed to preserve steady states are called well-balanced methods. Several well-balanced methods were proposed for one- and two-dimensional open-channel equations (open-channel flows) [e.g., LeVeque 2002; Capart et al. 2003; George 2006; Canestrelli et al. 2009], however most of these models force the preservation of “lake at rest” conditions by balancing the source term with the pressure gradient (local hydrostatic reconstruction). This approach may be reasonable for near or at “lake at rest” conditions but not necessarily in transient flow conditions (e.g., George 2006). In addition, some of these “well-balanced” methods may still lead to numerical storms if the slope of the conduit is relatively steep (e.g. 10%) even when a local hydrostatic reconstruction is used (e.g., George 2006). Furthermore, these “well-balanced” schemes work well in conduits where the top surface width does not significantly change with the water depth (e.g., rectangular or near-rectangular channels). For other cross-sections (e.g., circular, trapezoidal), these schemes may still lead to numerical storms. The latter is illustrated in Figure 1(a), in which, h_{rec} is the vertical water depth at the center of a cell (distance from bottom to free surface) and h_{mass} is the equivalent vertical water depth in the cell (uniform flow) that provides the same water volume as the “lake at rest”. For convenience, in the remainder of this paper the subscript *mass* is dropped. In a sloped circular conduit under “lake at rest” conditions, the water depth at the center of the cell from the horizontal water surface and that obtained from the hydraulic area A (water storage), do not coincide except when the horizontal water surface at the center of the cell (horizontal surface) is exactly half full. This lack of coincidence in a sloped pipe may lead to numerical storms if the scheme is not properly designed to preserve “lake at rest” conditions.

The model presented herein is an improved version of the model of Leon et al. (2010b). Only the new aspects of the model are presented herein. Two main contributions are made in the new model, namely: (1) a new method for water stage reconstruction that preserves “lake at rest” conditions regardless of the pipe slope and the pipe spatial discretization, (2) a horizontal system of coordinates instead of the commonly used inclined coordinate system (e.g., Capart et al. 1997; Bourdarias and Gerbi 2007; Leon et al. 2009 and 2010b) is used for facilitating the implementation of the proposed well-balanced scheme to complex conduit systems under transient and non-transient conditions. Five numerical test cases are presented and discussed.

GOVERNING EQUATIONS

The well-balanced method presented here is based on a two-governing equation model, where the open-channel region is simulated using the 1D Saint-Venant equations and the pressurized region is simulated using the 1D compressible waterhammer equations. A two-governing equation model has been shown to be suitable for minimizing numerical oscillations in pipe-filling bores for large waterhammer wave speeds (e.g., Leon and Ghidaoui 2010). Typically, the 1D Saint-Venant equations and the 1D compressible waterhammer equations are presented with reference to an inclined coordinate system x - z (see Figure 1) with x parallel to the conduit bottom (e.g., Chaudhry 1987, 2008; Leon et al. 2006, 2008, 2009). It is worth to mention that x - z is a local coordinate system for each conduit measured with respect to the local bottom (invert) of the conduit cross-section. The connection between conduits is made through boundary conditions. Most of the formulations for the 1D Saint-Venant equations and the 1D compressible waterhammer equations assume that the conduit slope is small and therefore $\cos \alpha$ (α = angle of inclination of the channel bottom) in the pressure term is set equal to unity. This is not the case for steep channels as $\cos \alpha$ may be significantly smaller than unity (1.0). Combining the notation of Bourdarias and Gerbi

(2007) and Leon et al. (2010b), the governing equations for prismatic conduits (the 1D Saint-Venant equations and the 1D compressible waterhammer equations) in the aforementioned inclined coordinate system x - z can be written in vector conservative form as

$$\frac{\partial \mathbf{U}}{\partial t} + \frac{\partial \mathbf{F}}{\partial x} = \mathbf{S} \quad (1)$$

where the vector variable \mathbf{U} , the flux vector \mathbf{F} and the source term vector \mathbf{S} are given by

$$\mathbf{U} = \begin{bmatrix} A_{eq} \\ Q_{eq} \end{bmatrix}, \mathbf{F} = \begin{bmatrix} Q_{eq} \\ \frac{Q_{eq}^2}{A_{eq}} + I_1 \cos \alpha \end{bmatrix} \text{ and } \mathbf{S} = \begin{bmatrix} 0 \\ (\sin \alpha - S_e)gA_{eq} \end{bmatrix} \quad (2)$$

where

$$A_{eq} = \begin{cases} A & \text{for open-channel flows} \\ \frac{\rho_f}{\rho_{ref}} A_{ref} & \text{for pressurized flows} \end{cases}, Q_{eq} = \begin{cases} Q & \text{for open-channel flows} \\ \frac{\rho_f}{\rho_{ref}} Q & \text{for pressurized flows} \end{cases}, I_1 = \begin{cases} \frac{A\bar{p}}{\rho_w} & \text{for open-channel flows} \\ \frac{A_{ref}p}{\rho_{ref}} & \text{for pressurized flows} \end{cases} \quad (3)$$

where the subscript eq stands for equivalent and it is used for depicting open channel and pressurized flow variables using a single representation. The variables for open-channel flows are: A = cross-sectional area of the flow; \bar{p} = average pressure of the water column over the cross sectional area; ρ_w = constant density for open-channel flows. The variables for compressible water hammer flows (pressurized flows) are: A_{ref} = reference hydraulic area, p = pressure acting on the center of gravity of A_{ref} , ρ_{ref} and p_{ref} are a reference density and reference pressure, respectively, and ρ_f = density for compressible water hammer flows (variable). Also, Q = flow discharge; g = gravitational acceleration, α = angle of inclination of the channel bottom and S_e

= slope of the energy line. The expressions for $\frac{A\bar{p}}{\rho_w}$ and $\frac{A_{ref}p}{\rho_{ref}}$ in the inclined coordinate system (circular cross-section) will not be used here and hence are not presented. However, the reader is referred to Leon et al. (2006, 2007, 2009, and 2010b) for these expressions. The reference state (*ref*) is defined at the change from open-channel to pressurized flow. This state is defined at an user-specified water depth (e.g., 95% of the maximum water depth in the cross-section). At this reference state all the flow parameters (e.g., fluid density, hydraulic area and average pressure) in both open-channel and pressurized flow regime are the same. Notice that $p_{ref} = \bar{p}_{ref}$ and $\rho_{ref} = \rho_w$. For convenience, in the remainder of this paper the subscript “*eq*” in A and Q used by Bourdarias and Gerbi (2007) are dropped.

The governing equations for prismatic conduits presented above are for the inclined coordinate system x - z . An actual system may have a large number of conduits and each of these may have a different angle of inclination (see Figure 2). Under “lake at rest” conditions, especially in complex pipe systems, it may be desirable to have a horizontal system of coordinates (\tilde{x} - \tilde{z}) rather than an inclined system because the flow depths in the horizontal system would be directly used in the local reconstruction of flow variables to achieve a well-balanced scheme. In this paper a horizontal system of coordinates is used for convenience in the aforementioned local reconstruction of flow variables. It is clear that the solution is independent of the coordinate system used. It is worth mentioning that if the conduit slope is steep, the $\cos \alpha$ term in Eq. (2) should be included regardless of the system of coordinates used (horizontal or inclined). The governing equations in the horizontal system of coordinates (\tilde{x} - \tilde{z}) can be written as (see Appendix A for derivation):

$$\frac{\partial \tilde{\mathbf{U}}}{\partial t} + \frac{\partial \tilde{\mathbf{F}}}{\partial \tilde{x}} = \tilde{\mathbf{S}} \quad (4)$$

where the vector variable $\tilde{\mathbf{U}}$, the flux vector $\tilde{\mathbf{F}}$ and the source term vector $\tilde{\mathbf{S}}$ are given by

$$\tilde{\mathbf{U}} = \begin{bmatrix} \tilde{A} \\ \tilde{Q} \end{bmatrix}, \quad \tilde{\mathbf{F}} = \begin{bmatrix} \tilde{Q} \\ \frac{\tilde{Q}^2}{\tilde{A}} + \tilde{I}_1 \cos^4 \alpha \end{bmatrix} \quad \text{and} \quad \tilde{\mathbf{S}} = \begin{bmatrix} 0 \\ (\sin \alpha - S_e)g\tilde{A} \cos \alpha \end{bmatrix} \quad (5)$$

The variables with a tilde “ \sim ” refer to the horizontal coordinate system. In Eq. (5), \tilde{A} is an estimate for the hydraulic area of cell i . This estimate is discussed in the section of treatment of source terms. For an inclined circular conduit, the vertical section becomes an ellipse. For an ellipse (Figure 1), the hydraulic area (A), and the term ($A\bar{p}/\rho$) are given by, respectively.

$$\tilde{A} = \begin{cases} ab(r\sqrt{1-r^2} + \arcsin r + \pi/2) & \text{for open-channel flows} \\ \frac{\rho_f}{\rho_{ref}} \tilde{A}_{ref} & \text{for pressurized flows} \end{cases} \quad (6)$$

$$\tilde{I}_1 = \begin{cases} \frac{\tilde{A}\bar{p}}{\rho} = 2gab \left[-\frac{1}{4}(b-h)\pi + \frac{1}{6}(\sqrt{1-r^2}(3hr + b(2-3r-2r^2)) - 3(b-h)\arcsin r) \right] & \text{for open-channel flows} \\ \frac{\tilde{A}_{ref}\tilde{p}}{\rho_{ref}} = \frac{\tilde{A}_{ref}\tilde{p}_{ref}}{\rho_{ref}} + c_f^2(\tilde{A} - \tilde{A}_{ref}) & \text{for pressurized flows (Leon et al. 2007)} \end{cases} \quad (7)$$

where c_f is the pressure wave celerity in pressurized flow conditions, $a = d/2$, $b = \frac{d}{2\cos \alpha}$, and $r = \frac{h}{b} - 1$ (see Figure 1). For estimating h (vertical water depth in open-channel or vertical piezometric head with reference to the conduit bottom in surcharged flow conditions), an iterative procedure is required for open-channel flow conditions while as an explicit expression can be obtained for pressurized flows. Here, for open-channel flows, h is obtained from \tilde{A} (Eq. 6) by using the Newton-Raphson root finding method. The derivative of \tilde{A} (with respect to r) that is needed when using the Newton-Raphson

iterative method is given by

$$d\tilde{A}/dr = 2ab\sqrt{1-r^2} \quad (8)$$

For pressurized flows, h is obtained from Eq. (7) which gives

$$h = h_{ref} + \frac{c_f^2}{g} \left(\frac{\tilde{A}}{\tilde{A}_{ref}} - 1 \right) \quad (9)$$

In Eq. (5), S_e doesn't have a tilde because it is computed in the inclined rather than in the horizontal system of coordinates. This is due to numerical efficiency given that the computation of the wetted perimeter p_w , which in turn is required for the computation of S_e , involves elliptical integrals in the horizontal system of coordinates. Elliptical integrals can be solved by numerical integration only, and hence they are computationally expensive. To avoid the computation of elliptic integrals, S_e is determined exactly in the $x - z$ system of coordinates (circular conduit) using a water depth equal to $h \cos \alpha$ for open-channel flows and a piezometric head equal to $h_{ref} \cos \alpha$ for surcharged flows. Manning's equation is used for computing the slope of the energy line as follows:

$$S_e = \frac{n_m^2 \frac{Q}{A} \left| \frac{Q}{A} \right|}{k_n^2 R^{4/3}} \quad (10)$$

where k_n is 1.0 in Metric units and 1.49 in English units, n_m is the Manning roughness coefficient and again, A and R are computed using a circular cross-section (see Leon et al. 2006).

NUMERICAL SCHEME

For a better illustration of the proposed well-balanced scheme, a pseudocode of the scheme is presented in Appendix B. The explicit Godunov-type finite volume method (e.g., Leveque 2002) is used to update the solution in cell i from the n to the $n + 1$ time

level as

$$\tilde{\mathbf{U}}_i^{n+1} = \tilde{\mathbf{U}}_i^{n+1/2} + \Delta t \mathbf{S}_i^{n+1/2} \quad (11)$$

where

$$\tilde{\mathbf{U}}_i^{n+1/2} = \tilde{\mathbf{U}}_i^n - \frac{\Delta t}{\Delta \tilde{x}} (\tilde{\mathbf{F}}_{i+1/2}^n - \tilde{\mathbf{F}}_{i-1/2}^n) \quad (12)$$

and $\mathbf{S}_i^{n+1/2}$ is computed using $\tilde{\mathbf{U}}_i^{n+1/2}$. In the equations above, $\Delta \tilde{x}$ is the length of the cell in the \tilde{x} axis of the horizontal system of coordinates, Δt is the time step and the i th cell is centered at node i and extends from $i - 1/2$ to $i + 1/2$. The flow variables $\tilde{\mathbf{U}}$ (\tilde{A} and \tilde{Q}) are defined at cell centers i and represent their average value within each cell. Fluxes, on the other hand are evaluated at the interfaces between cells ($i - 1/2$ and $i + 1/2$). Note in Eq. (11) that the source terms are introduced into the solution through time splitting. The treatment of the gravity ($\sin \alpha \cos \alpha g \tilde{A}$) and friction ($S_{ef} \tilde{A} \cos \alpha$) source terms are discussed later in the section ‘‘Treatment of source terms and stationarity’’.

RECONSTRUCTION OF FLOW VARIABLES AND INTERNAL FLUXES

In a similar way to Leon et al. (2010b), the Monotone Upstream-centred Scheme for Conservation Laws (MUSCL) reconstruction in conjunction with the Hancock two-stage scheme (e.g., Toro 2001) is used for advancing (from one time level to the next) the cell average solution of the variable \tilde{A} but not of \tilde{Q} . For the variable \tilde{Q} , a constant flow discharge is used at each cell. Attempting to use the MUSCL-Hancock method for \tilde{Q} may result in numerical storms when the the flow is near or at ‘‘lake at rest’’ conditions. The reason for the latter is due to the fact that in sloped pipes under ‘‘lake at rest’’ conditions, the spatial gradient of the pressure term in the governing equations $\partial/\partial \tilde{x}(\tilde{A}_{ref} \tilde{p}_{ref}/\rho_{ref})$ is not constant but a function of the local water depth (see Eq. 5).

For the reconstruction of the variable \tilde{A} (to be used in the MUSCL-Hancock method), most ‘‘well-balanced schemes’’ use the water stage at the center of a cell ($\eta_i = h_i + z_{bi}$)

where h_i is obtained directly from the cell averaged value of \tilde{A}_i . The latter approach for the reconstruction of water stage ($\eta_i = h_i + z_{bi}$) may still lead to numerical storms under near or at “lake at rest” conditions even when the aforementioned local hydrostatic reconstruction is used. In a sloped pipe under “lake at rest” and open-channel flow conditions, the water depth at the center of the cell from the horizontal water surface and that obtained from the cell averaged \tilde{A} (water storage), do not coincide except when the horizontal water surface at the center of the cell (horizontal surface) is exactly half full. This lack of coincidence is only for open-channel flows but not for pressurized flows. The lack of coincidence in a sloped pipe under “lake at rest” and open-channel flow conditions occurs in all cross-sections except in rectangular channels and may lead to numerical storms especially for steep slopes and for long simulation periods (e.g., continuous simulations). To avoid numerical storms created by this lack of coincidence, a reconstruction of the water surface based on a horizontal water surface in each cell is used. This approach was used before over arbitrary topography with wetting and drying by Begnudelli and Sanders (2006) and for sloped sewer pipes by Sanders and Bradford (2011). The water depth (or water stage) obtained from this reconstruction is not the same as that obtained directly from the cell averaged value of \tilde{A} . \tilde{A}_i is a strict measure of water storage ($\tilde{A}\Delta\tilde{x}_i$), which is important for ensuring conservation of mass. For determining the water stage at the center of a cell using the proposed reconstruction, it is necessary to find a relationship between this water depth (or at the cell boundaries) and the volume of water in a sloped pipe under “lake at rest” conditions. This volume V between two vertical sections for open-channel flows is given by

$$V = \frac{ab^2}{6 \tan \alpha} \left[\left(3\pi r_2 + 2\sqrt{1 - r_2^2} (2 + r_2^2) + 6r_2 \arcsin r_2 \right) - \left(3\pi r_1 + 2\sqrt{1 - r_1^2} (2 + r_1^2) + 6r_1 \arcsin r_1 \right) \right] \quad (13)$$

where $r_1 = \frac{h_1}{b} - 1$, $r_2 = \frac{h_1 + \Delta\tilde{x} \tan \alpha}{b} - 1$, and h_1 is the vertical water depth at the left of the cell. For computing r_1 ($-1 \leq r_1 \leq 1$) and hence h_1 , the Newton-Raphson root finding method is used. The function is given by $f_V = V - \tilde{A}\Delta\tilde{x}$. The derivative of f_V with respect to r_1 is given by

$$\frac{df_V}{dr_1} = \frac{ab^2}{\tan \alpha} \left[r_2 \sqrt{1 - r_2^2} - \arccos r_2 - \left(r_1 \sqrt{1 - r_1^2} - \arccos r_1 \right) \right] \quad (14)$$

The water depth at the center of a cell for reconstruction is given by $h_{rec} = (r_1 + 1)b + \frac{\Delta z_b}{2}$. This type of reconstruction for the water depth ensures a horizontal water surface under “lake at rest” conditions, while \tilde{A} ensures a strict conservation of mass. For surcharged flows (see Figure 3), $h_{rec_i} = h_i$ (Eq. 9) because the piezometric head at the center of a cell determined from a horizontal water surface and that obtained from the cell averaged \tilde{A} are the same. For partial open channel - partial surcharged flow conditions, the water stage is obtained from the cell volume, which is given by the sum of an identical expression to Eq. (13) with $\Delta\tilde{x}_1$ (open channel region) and $\tilde{A}\Delta\tilde{x}_2$ (surcharged region), where $\Delta\tilde{x} = \Delta\tilde{x}_1 + \Delta\tilde{x}_2$.

To avoid spurious oscillations, the MINMOD flux limiter is used here. The two arguments for the MINMOD function are $\frac{z_{b_i} + h_{rec_i}^n - (z_{b_{i-1}} + h_{rec_{i-1}}^n)}{\Delta\tilde{x}}$ and $\frac{z_{b_{i+1}} + h_{rec_{i+1}}^n - (z_{b_i} + h_{rec_i}^n)}{\Delta\tilde{x}}$. Then, the MINMOD function of these two arguments is determined as usual (e.g., LeVeque 2002)

$$\text{minmod}(a, b) = \begin{cases} a & \text{if } |a| < |b| \text{ and } ab > 0, \\ b & \text{if } |b| < |a| \text{ and } ab > 0, \\ 0 & \text{if } ab \leq 0 \end{cases} \quad (15)$$

This reconstruction is intended for relatively steep slopes and when the flow is near or at “lake at rest” conditions. For mild slopes or when the flow is not near nor at “lake at rest” conditions, the reconstruction of the water stage can be obtained directly from

\tilde{A} using Eq. (6) or Eq. (9), depending on if the flow is open channel or surcharged, respectively.

TREATMENT OF SOURCE TERMS AND STATIONARITY

Regardless of the reconstruction approach for the flow variables (in this case only \tilde{A}), it is well known that schemes that introduce source terms into the solution through time splitting generally don't preserve "lake at rest" conditions in time. For preserving the "lake at rest" conditions, several approaches based mainly on a local hydrostatic reconstruction were proposed (e.g., LeVeque 1998, Capart et al. 2003). The later means that if the water in a sloped pipe is motionless (u [velocity] ≈ 0), the pressure gradient in Eqs. (2) and (5) must be balanced by the gravity source term. This leads to the following estimate for \tilde{A} in Eqs. (2) and (5)

$$\tilde{A} = -\cos^2 \alpha \frac{\left(\frac{\tilde{A}\tilde{p}}{\rho}\right)_R - \left(\frac{\tilde{A}\tilde{p}}{\rho}\right)_L}{g(z_{bR} - z_{bL})} \quad (16)$$

The above estimate for \tilde{A} would be appropriate when the water is near or at "lake at rest" conditions, however this may be inappropriate for flows that are far from these conditions. Hence an estimate for \tilde{A} in Eqs. (2) and (5) that would be appropriate in rest and non-rest conditions is sought. An estimate that satisfies these conditions can be obtained by applying the Leibnitz's rule to the pressure gradient term (see Appendix C), which gives

$$\tilde{A} \approx \cos^2 \alpha \frac{\left(\frac{\tilde{A}\tilde{p}}{\rho}\right)_R - \left(\frac{\tilde{A}\tilde{p}}{\rho}\right)_L}{g(h_R - h_L)} \quad (17)$$

Note that in water at rest conditions $h_R - h_L = -(z_{bR} - z_{bL})$ and hence Eqs. (16) and (17) are identical. This implies that the proposed estimate for \tilde{A} in Eq. (17) and hence for the gravity source term is more general than that obtained balancing the pressure gradient and the gravity source term. Finally, the source term \mathbf{S} can be written as

$$\mathbf{S}_i^{n+1/2} = (\sin \alpha - S_e^{n+1/2}) g \bar{A}^{\approx n+1/2} \cos \alpha \quad (18)$$

where

$$S_e^{n+1/2} = \frac{n_m^2 \left(\frac{Q}{A}\right)^{n+1/2} \left|\frac{Q}{A}\right|^{n+1/2}}{k_n^2 (R^{4/3})^{n+1/2}} \quad (19)$$

TREATMENT OF BOUNDARY CONDITIONS

The treatment of boundary conditions for the model presented here is the same as that described in Leon et al. (2010a). It is clear that the variables in the horizontal system of coordinates rather than in the inclined system must be used.

NUMERICAL TESTS

The purpose of this section is to test the accuracy of the proposed well-balanced scheme for various flow conditions. Five tests cases are considered as follows:

Test 1: Stationarity

The purpose of this test is to demonstrate the capability of the proposed scheme in preserving “lake at rest” conditions (stationarity). This test, which is depicted in Figure 4, is comprised of a two circular conduit system forming a pool of still water adjacent to dry regions (wet-dry bed interfaces). Each of the conduits are 50 m long and have a diameter of 5.0 m and a Manning roughness coefficient of 0.015. The longitudinal slope of the conduit on the left is -10% while as the conduit on the right is +10%. The simulations were performed using 12 cells in each conduit and a Courant number (Cr) of 0.80 for both conduits. It is worth mentioning that explicit schemes are stable for Courant numbers less than or equal to one, however it is common practice to use a Cr significantly smaller than one for numerical stability reasons. Numerical instabilities may occur under rapid flow acceleration conditions (e.g., sudden increase in flow velocity), when the distance of wave propagation in one time step exceeds $\Delta \tilde{x}$.

The boundary conditions used for this test are zero water flux conditions, which is $Q(x = 0, t) = 0$ and $Q(x = 100, t) = 0$. The initial conditions are:

$$\begin{cases} z_{bi} + h_{rec_i} = 4.0 \text{ m and } u = 0 \text{ m/s for } 10 \text{ m} < x < 90 \text{ m} \\ h = 0 \text{ m and } u = 0 \text{ m/s for } x \leq 10 \text{ m and } x \geq 90 \text{ m} \end{cases}$$

The initial conditions above show a pool of still water adjacent to dry regions. This test aims to evaluate if the scheme preserves in time the initial conditions. The solution was integrated for 10^3 , 10^5 and 10^7 time steps using a precision for the water depth of $10^{-8}m$. Table 1 presents the maximum discharge and the maximum water depth fluctuation (with respect to the initial conditions) attained at the end of each simulation. The results in Table 1 indicate that the proposed scheme preserves steady states at the computer precision used.

Even though, the “lake at rest” condition is the simplest case of a steady state flow, this condition may produce numerical storms if not handled properly. To illustrate this, Figure 5 shows the dimensionless flow discharge $[Q/(gd^5)^{1/2}]$ versus number of time steps (Nr) at midway of first conduit for the present model and an earlier model of the first author that doesn’t have a treatment for “lake at rest” conditions (Leon et al. 2010b). As can be observed in Figure 5, unlike the model of Leon et al. (2010b) that oscillates with time, the present model preserves “lake at rest” conditions ($Q = 0$). Note that the amplitude of the oscillations obtained with the model of Leon et al. (2010b) decays with time (due to friction) and converges to a finite value different from zero.

Test 2: Steady-State flows

The purpose of this test is to demonstrate the capability of the proposed scheme in preserving steady-state flows. This test, which is depicted in Figure 6, is comprised of a three circular conduit system. The Manning roughness coefficient and diameter for all pipes are 0.015 and 1 m, respectively. The length of the conduits, from left to right

are, 50 m, 300 m and 50 m, respectively. The longitudinal slope of the conduits, from left to right are, 5%, 0.1667% and 5%, respectively. The simulations were performed using 40 cells in the shortest conduit and a Cr of 0.80 for all conduits. The boundary conditions used for this test are $Q(x = 0, t) = 0.44 \text{ m}^3/\text{s}$ and $h(x = 0, t) = 0.20 \text{ m}$. The initial conditions ($t = 0$) are $h = 0.05 \text{ m}$ and $Q = 0 \text{ m}^3/\text{s}$ for $x > 0 \text{ m}$.

The water surface profile in the system after 500 seconds is presented in Figure 6. The normal depths for each of the conduits are also presented in this Figure. The flow depth and discharge at midway of second conduit from left are presented in Figures 7 and 8, respectively. As can be observed in Figures 6 - 8, the present model resolves well steady states. In particular, note in Figures 7 and 8 that the water depth and flow discharge remain invariant with time after steady state is achieved.

Test 3: dry-wet bed flow conditions

The purpose of this test is to demonstrate the capability of the proposed scheme in attaining and preserving “lake at rest” conditions when the flow is adjacent to dry regions (wet-dry bed interfaces). Test 3 is comprised of a two circular conduit system that is partially in open-channel flow conditions and partially in dry-bed flow conditions (see Figure 9). Each of the conduits are 50 m long and have a diameter of 5.0 m and a Manning roughness coefficient of 0.015. The longitudinal slope of the conduit on the left is -5% while as the conduit on the right is +5%. The simulations were performed using 20 cells in each conduit and a Courant number (Cr) of 0.80 for both conduits. This test simulates the sudden opening of a gate separating one pool of still water (left conduit) and the right conduit completely dry (see Figure 9). The boundary conditions used for this test are zero water flux conditions, which is $Q(x = 0, t) = 0$

and $Q(x = 100, t) = 0$. The initial conditions are:

$$\begin{cases} z_{bi} + h_{rec_i} = 2.5 \text{ m and } u = 0 \text{ m/s for } x \leq 50 \text{ m} \\ h = 0 \text{ m and } u = 0 \text{ m/s for } x > 50 \text{ m} \end{cases}$$

At time $t = 0$, the gate is instantaneously opened which generates a shock wave moving to the right and a rarefaction wave moving to the left. The simulation results for the water surface profiles at various times are shown in Figures (9) through (12). The results for the water depth, flow velocity and flow discharge traces at midway of both conduits are depicted in Figures (13), (14) and (15), respectively. The results in Figures (13) through (15) indicate that the system achieves “lake at rest” conditions at about $t = 500$ seconds. These figures also show that the “lake at rest” conditions are preserved in time.

Test 4: partial open channel-partial surcharged flow conditions

The purpose of this test is to demonstrate the capability of the proposed scheme in attaining and preserving “lake at rest” conditions when the flow is under partial open channel and partial surcharged flow conditions. As in test case 1, this test simulates the sudden opening of a gate separating one surcharged pool of still water (left conduit) and the right conduit completely dry. The left conduit is 100 m long and the right conduit is 70 m long. Both conduits have a diameter of 5.0 m and a Manning roughness coefficient of 0.015. The longitudinal slope of the conduit on the left is -5% while as the conduit on the right is +5%. The pressure wave celerity used for surcharged flow conditions is 100 m/s. The simulations were performed using 58 cells in the left conduit and 40 cells in the right conduit and a Cr of 0.80 for both conduits. The boundary conditions used for this test case are the same as those used for Test 3 (zero

water flux conditions). The initial conditions are:

$$\begin{cases} z_{bi} + h_{rec_i} = 20 \text{ m and } u = 0 \text{ m/s for } x \leq 100 \text{ m} \\ h = 0 \text{ m and } u = 0 \text{ m/s for } x > 100 \text{ m} \end{cases}$$

At time $t = 0$, the gate is instantaneously opened. The results for the piezometric depth, flow velocity and flow discharge traces at midway of both conduits are depicted in Figures (16), (17) and (18), respectively. The time axis of Figures (17) and (18) were limited to 1500 seconds for clarity purposes, however the results show that the system attains “lake at rest” conditions ($u < 1 \text{ cm/s}$) at about $t = 2000$ seconds. Note that Figures (16) through (18) show a slow convergence to “lake at rest” conditions. In an actual case, the system will likely attain “lake at rest” conditions in a shorter time ($t < 2000 \text{ s}$). This discrepancy is because the model doesn’t consider unsteady friction.

Test 5: Experiment of Vasconcelos et al. 2006

The purpose of this test is to demonstrate the ability of the proposed model to reproduce experimental surcharged flow conditions for relatively steep slopes. The experimental work of Vasconcelos et al. (2006) is used because the experimental work was performed using conduits with slopes of 2%. The experimental setup consisted of an acrylic pipeline 14.33 m long, having an inner diameter of 9.4 cm. The center portion of this pipe was raised about 15 cm with respect to both ends in order to create conditions for the occurrence of sub-atmospheric pressures. The pipeline was connected at its upstream end by a box tank and by a cylindrical tank at its downstream end. The experiment considered was obtained by filling the system to a level of 0.30 m at the box tank and the system allowed to come to rest. Then a syphon outflow was suddenly initiated at the box tank ($t = 0$). After some time, the water level in the box tank decreased to a level that created sub-atmospheric pressures at the center portion of the pipe. When the water level at the box tank dropped below the pipe crown, a com-

plex flow pattern was developed. In this case, the flow just downstream of the box tank was in sub-atmospheric conditions, and under these conditions, air flow flowed from the tank into the pipe. This constitutes a two-phase flow problem that is outside of the scope of this work. The intrusion of air flow in the experiment occurred at about $t = 42.5$ s, and in the model about 1.7 seconds earlier. Since our work is limited to single-phase flows, the comparison between model prediction and experimental results are presented until right before the occurrence of air intrusion only ($t < \approx 40.8$ s).

To show the sequence of the formation of sub-atmospheric pressures, simulated piezometric depth snapshots at different times are presented in Fig. 19. When using the present model to simulate fully pressurized flows, as in this test case, A_{ref} can be set equal to A_f (full cross-sectional area of the conduit). The pressure wave celerity used in the simulations was 300 m/s based on experimental measurements of pressure pulse propagation. The outflow was assumed constant and a value of 0.45 L/s was estimated by observing the change in water volume over time. For estimating energy losses, Vasconcelos et al. (2006) used a Manning roughness coefficient of 0.012, which was also used here.

The simulated and experimental velocities at 9.9 m downstream of the box tank are presented in Fig. 20. The model predictions and experiments for the piezometric depth at 14.1 m downstream of the box tank are presented in Fig. 21. The simulated results were generated using 400 cells and a Cr of 0.80. The results for the velocities (Fig. 20) show good agreement between model and experiments for the frequency of oscillations. However, the velocity amplitudes are overestimated by the model. As suggested by Vasconcelos et al. (2006), this may be in part because the outflow uniformity assumption may not be accurate. The differences between model prediction and experiments may be associated also to neglecting minor losses and unsteady friction in the model. The results for the piezometric depth (Fig. 21) show a good agreement

between model predictions and experiments. The differences between the simulated and experimental piezometric depths may be explained using the same reasons given for the velocities.

CONCLUSIONS

The model presented herein is the same as that of Leon et al. (2010b), except that it has been modified to preserve “lake at rest” conditions in sloped prismatic conduits. The results of the new model (present paper) are identical to those of Leon et al. (2010b) for non-rest conditions. These schemes are based on the two-governing equation model, where open channel flows are simulated using the Saint-Venant equations and pressurized flows using the compressible water hammer equations. The key findings are as follows:

1. Results show that the proposed model attains and preserves “lake at rest” conditions (horizontal still water) for steep slopes when the flow is adjacent to dry regions (wet-dry bed interfaces) and under partial open-channel and partial surcharged flow conditions, and under fully surcharged flow conditions. No simulation presented characteristics of “numerical storms”.
2. Results also show that the model resolves moving jump discontinuities (e.g., shocks) even when adjacent to dry regions.
3. The results also show a good agreement between model predictions and experiments for fully surcharged flow conditions. Overall, the proposed model attains and preserves “lake at rest” conditions regardless of the conduit slope, resolves moving jump discontinuities over dry-beds in sloped conduits, and resolves small perturbations from steady-states, even when adjacent to dry regions.

ACKNOWLEDGMENTS

The authors gratefully acknowledge the financial support of the School of Civil

and Construction Engineering at Oregon State University (OSU) and Northwest Hydraulic Consultants (NHC), Pasadena, CA. The authors also gratefully acknowledge Drs. David Axworthy, Mohamed Ghidaoui and Arthur Schmidt for providing insightful comments and suggestions during the preparation of the manuscript. Last but not least, the authors are indebted to the anonymous reviewers for their insight, constructive criticisms and suggestions on an earlier version of the manuscript.

APPENDIX A

This Appendix presents the transformation of the continuity and momentum equations from the inclined x - z coordinate to the horizontal system \tilde{x} - \tilde{z} (See Figure 1). Herein we follow the method of Chaudhry (2008) for transformation of coordinates of the two-dimensional shallow water (open-channel) equations. Notice that this transformation involves only a rotation around a fixed point. The transformation matrix for this rotation is given as (presented in most books of Algebra),

$$\begin{bmatrix} \cos \alpha & + \sin \alpha \\ - \sin \alpha & \cos \alpha \end{bmatrix} \quad (20)$$

Using Eq. (20), the functional form for \tilde{x} and \tilde{z} (new coordinates) and x and z (old coordinates) are given by

$$\begin{bmatrix} \tilde{x} \\ \tilde{z} \end{bmatrix} = \begin{bmatrix} \cos \alpha & + \sin \alpha \\ - \sin \alpha & \cos \alpha \end{bmatrix} \begin{bmatrix} x \\ z \end{bmatrix} \quad (21)$$

$$\begin{bmatrix} x \\ z \end{bmatrix} = \begin{bmatrix} \cos \alpha & - \sin \alpha \\ \sin \alpha & \cos \alpha \end{bmatrix} \begin{bmatrix} \tilde{x} \\ \tilde{z} \end{bmatrix} \quad (22)$$

The transformed variables in the new coordinate system become (see Figure 1)

$$\begin{aligned}
 h &= y / \cos \alpha \\
 \tilde{A} &= A / \cos \alpha \\
 \tilde{Q} &= Q \\
 \tilde{p} &= \bar{p} / \cos \alpha
 \end{aligned} \tag{23}$$

in which h is the vertical flow depth (open-channel) or piezometric head with reference to the conduit bottom (surcharged flow) measured vertically and the variables with a “~” are referred to the \tilde{x} - \tilde{z} system of coordinates. Also, according to Eq. (21)

$$\frac{\partial}{\partial x} = \cos \alpha \frac{\partial}{\partial \tilde{x}} - \sin \alpha \frac{\partial}{\partial \tilde{z}} \tag{24}$$

The term containing the \tilde{z} derivative in Eq. (24) is undesirable, since the original equations of continuity and momentum have a single spatial dimension (x). However, the ratio of the second term on the right-hand side in Eq. (24) compared to the first term on the right-hand side in the same equation gives $\tan^2 \alpha$, which is negligible. The reader can notice that although $\sin \alpha$ may not be small, the terms $\sin^2 \alpha$ and $\tan^2 \alpha$ are small and hence can be dropped. The introduction of Eqs. (23) and (24) into the continuity and momentum equations in the inclined coordinates (Eq. 2) give

$$\mathbf{U} = \begin{bmatrix} \tilde{A} \\ \tilde{Q} \end{bmatrix}, \mathbf{F} = \begin{bmatrix} \tilde{Q} \\ \frac{\tilde{Q}^2}{\tilde{A}} + \cos^4 \alpha \frac{\tilde{A} \tilde{p}}{\rho} \end{bmatrix} \text{ and } \mathbf{S} = \begin{bmatrix} 0 \\ (\sin \alpha - S_e) g \tilde{A} \cos \alpha \end{bmatrix} \tag{25}$$

APPENDIX B

Pseudocode for well-balanced scheme

- 1: **Specify** required data and parameters [e.g., pipe geometry, boundary conditions (BCs), calculation parameters]
 - 2: $t = 0, n = 0$
 - 3: **Read** initial flow variables at the center of all cells h_i^n, \tilde{A}_i^n and \tilde{Q}_i^n
 - 4: **while** ($t \leq$ period of simulation) **do**
 - 5: **Compute** maximum Δt based on specified Courant number and flow variables at the center of each cell
 - 6: **Compute** $\tilde{A}^{n+1/2}$ and $\tilde{Q}^{n+1/2}$ at the boundaries of each conduit using flow variables at time level n and specified boundary conditions {Depending on BC, use Eqs. (1)-(11) in Leon et al. (2010a)}
 - 7: **Compute** η_L (\tilde{A}_L) and η_R (\tilde{A}_R) for each cell by performing a water stage reconstruction. {No reconstruction of Q is performed (see reconstruction of flow variables section in this paper)}
 - 8: **Apply** the MINMOD flux limiter at all cell interfaces (e.g., $i - 1/2, i + 1/2$) to avoid spurious oscillations [e.g., at $x = i + 1/2$, apply MINMOD ($\eta_{R_i}, \eta_{L_{i+1}}$)]. {Use Eq. (15) in this paper}
 - 9: **Solve** Riemann problem at all cell interfaces, i.e., compute h, \tilde{A} and \tilde{Q} at each cell interface. {Use Eqs. (6)-(8) in Leon et al. 2009 for pure open-channel flow interfaces, Eqs. (13)-(14) in Leon et al. 2008 for pure pressurized flow interfaces, and Eqs. (12)-(20) in Leon et al. 2010b for mixed flow interfaces.}
 - 10: **Compute** fluxes at all cell interfaces using Eqs. (5)-(7) in this paper with h, \tilde{A} and \tilde{Q} determined at the previous step.
 - 11: **Compute** the source terms for each cell. {Use Eqs. (16)-(19) in this paper}
 - 12: **Update** the solution in all cells using Eq. (11) in this paper.
 - 13: $t = t + \Delta t; n = n + 1$
 - 14: **end while**
-

APPENDIX C

In this Appendix, part of the pressure term in the momentum equation ($\partial/\partial\tilde{x}[(\tilde{A}\tilde{p})/\rho]$) is mathematically manipulated to find an estimate for \tilde{A} (Eq. 5).

Let's start expressing the term $\partial/\partial\tilde{x}[(\tilde{A}\tilde{p})/\rho]$ as a function of the terms ξ , \tilde{z} and h (see Figure 1)

$$\frac{\partial}{\partial\tilde{x}}\left(\frac{\tilde{A}\tilde{p}}{\rho}\right) = g\frac{\partial}{\partial\tilde{x}}\left(\int_0^{h(\tilde{x})}\xi(\tilde{z})(h(\tilde{x})-\tilde{z})d\tilde{z}\right) \quad (26)$$

Note in Eq. (26) that the integral is the first moment of the area with respect to the water surface. Denoting the term $\xi(\tilde{z})(h(\tilde{x})-\tilde{z})$ as $F(\tilde{z}, \tilde{x})$, the term $\partial/\partial\tilde{x}[(\tilde{A}\tilde{p})/\rho]$ becomes

$$\frac{\partial}{\partial\tilde{x}}\left(\frac{\tilde{A}\tilde{p}}{\rho}\right) = g\frac{\partial}{\partial\tilde{x}}\left(\int_0^{h(\tilde{x})}F(\tilde{z}, \tilde{x})d\tilde{z}\right) = g\frac{\partial\Psi(\tilde{z}, \tilde{x})}{\partial\tilde{x}} \quad (27)$$

The Leibnitz's rule in terms of the variables \tilde{x} and \tilde{z} (see Figure 1) is given by

$$\frac{d}{d\tilde{x}}\int_{f_1(\tilde{x})}^{f_2(\tilde{x})}F(\tilde{z}, \tilde{x})d\tilde{z} = \int_{f_1(\tilde{x})}^{f_2(\tilde{x})}\frac{\partial}{\partial\tilde{x}}F(\tilde{z}, \tilde{x})d\tilde{z} + F(f_2(\tilde{x}), \tilde{x})\frac{df_2}{d\tilde{x}} - F(f_1(\tilde{x}), \tilde{x})\frac{df_1}{d\tilde{x}} \quad (28)$$

Note that the operator in the Leibnitz's rule (left-hand side) is a total derivative, while as the operator in Eq. (27) is a partial derivative. Because Ψ is a function of \tilde{z} and \tilde{x} , the total derivative of $\Psi(\tilde{z}, \tilde{x})$ with respect to \tilde{x} can be written as

$$\frac{d\Psi}{d\tilde{x}} = \frac{\partial\Psi}{\partial\tilde{x}} + \frac{\partial\Psi}{\partial\tilde{z}}\frac{d\tilde{z}}{d\tilde{x}} \quad (29)$$

Given that \tilde{z} is independent of \tilde{x} , $d\Psi/d\tilde{x} = \partial\Psi/\partial\tilde{x}$ (Eq. 29). Now, we can apply the Leibnitz's rule to the right hand side of Eq. (27), which gives,

$$\frac{\partial}{\partial\tilde{x}}\left(\frac{\tilde{A}\tilde{p}}{\rho}\right) = g\tilde{A}\frac{\partial h}{\partial\tilde{x}} \quad (30)$$

It is acknowledged that Chaudhry (1987) has obtained a similar relation to Eq. (30)

based on a Taylor series expansion neglecting higher-order terms. The reader can note that in the derivation presented above no terms were neglected and the equation is valid regardless of the flow velocity (e.g., steady state, water at rest or moving jump discontinuities). Equation (30) can be written as

$$\tilde{A} = \frac{1}{g} \frac{\partial}{\partial \tilde{x}} \left(\frac{\tilde{A}\tilde{p}}{\rho} \right) / \frac{\partial h}{\partial \tilde{x}} \quad (31)$$

Note that multiplying both sides of Eq. (31) by $\cos^2 \alpha$, it can be obtained a similar expression to Eq. (16). Denoting $\tilde{A} \cos^2 \alpha$ as \hat{A} , Eq. (31) can be written as

$$\hat{A} = \cos^2 \alpha \frac{\left(\frac{\tilde{A}\tilde{p}}{\rho} \right)_R - \left(\frac{\tilde{A}\tilde{p}}{\rho} \right)_L}{g(h_R - h_L)} \quad (32)$$

The expression of \hat{A} in Eq. (32) is recommended as an estimate for \tilde{A} in Eq. (5).

NOTATION

The following symbols are used in this paper:

A = cross-sectional area of flow;

$a = d/2$;

$b = d/(2 \cos \alpha)$;

c = gravity wave celerity;

c_f = waterhammer wave celerity;

Cr_{max} or Cr = maximum Courant number;

d = conduit diameter;

\mathbf{F} = Flux vector;

$\mathbf{F}_{i+1/2}^n$ = intercell flux;

g = gravitational acceleration;

h = water depth or piezometric head above channel bottom in \tilde{z} direction;

h_{rec} = vertical water depth (or piezometric head above channel bottom) at the center of a cell;

h_{mass} = equivalent vertical water depth in the cell (uniform flow) that provides the same water volume as the “lake at rest” condition;

\bar{h} = vertical distance from the conduit invert to the centroid of the hydraulic area;

k_n = constant equal to 1.0 in Metric units and 1.49 in English units;

n_m = Manning roughness coefficient;

Nr = Number of time steps;

p = pressure acting on the center of gravity of A_{ref} ;

\bar{p} = average pressure of the water column over the cross sectional area;

Q = flow discharge;

R = hydraulic radius;

$r = h/b - 1$;

\mathbf{S} = vector containing source terms;

S_e = slope of the energy line;

S_o = bed slope;

t = time;

\mathbf{U} = vector of flow variables;

u = water velocity;

V = water volume;

x = longitudinal coordinate parallel to the conduit bottom;

\tilde{x} = horizontal axis;

y = water depth or piezometric head above channel bottom in z direction;

z = axis perpendicular to x ;

\tilde{z} = vertical axis perpendicular to \tilde{x} ;

\tilde{z}_b = elevation of channel bottom;

α = angle of inclination of the channel bottom;

Δx = spatial mesh size in x direction;

$\Delta \tilde{x}$ = spatial mesh size in \tilde{x} direction;

Δt = time step;

η = water stage;

ρ_f = density for compressible water hammer flows (variable);

ρ_w = density for open-channel flows (constant)

Superscripts

n = computational time level

Subscripts

eq = equivalent;

i = mesh point location in x direction;

L = left state;

R = right state;

ref = reference

REFERENCES

Begnudelli, L. and Sanders, B.F. (2006). Unstructured Grid Finite Volume Algorithm for Shallow-water Flow and Transport with Wetting and Drying. *J. Hydraulic Engng.* 132(4), 371-384.

Bourdarias, C., Gerbi, S. (2007). A finite volume scheme for a model coupling free surface and pressurised flows in pipes. *J. Computational and Applied Mathematics*, 209(1), 109-131.

Caleffi, V., Valiani, A., and Zanni, A. (2003). Finite Volume method for simulating extreme flood events in natural channels. *J. Hydraul. Research*, 41(2), 167-177.

Canestrelli, A., Siviglia, A., Dumbser, M., and Toro, E. F. (2009). Well-balanced high-order centred schemes for non-conservative hyperbolic systems. Applications to

shallow water equations with fixed and mobile bed, *Adv Water Res.* 32(6), 834-844.

Capart, H., Sillen, X., Zech Y. (1997). Numerical and experimental water transients in sewer pipes. *J. Hydraul. Research*, 35(5), 659-672.

Capart, H., Eldho, T.I., Huang, S.Y., Young, D.L., and Zech Y. (2003). Treatment of natural geometry in finite volume river flow computations. *J. Hydraulic Engng.* 129 (5), 385-393.

Cardle, J.A. (1984). An investigation of hydraulic transients in combination of free surface and pressurized flows. PhD thesis. Dept. of Civil and Mineral Engng., Univ. of Minnesota, Twin Cities MN.

Cardle, J.A., Song, C.C.S. (1988). Mathematical modeling of unsteady flow in storm sewers. *Int. J. of Engng. Fluid Mechanics*, 1(4), 495-518.

Chaudhry, M. H. (1987). *Applied hydraulic transients*, Van Nostrand Reinhold, New York.

Chaudhry, M. H. (2008). *Open-channel flow*, 2nd edition, Springer-Verlag New York.

George, D. L. (2006). Finite Volume Methods and Adaptive Refinement for Tsunami Propagation and Inundation. PhD thesis. Dept. of Applied Mathematics, Univ. of Washington, Seattle, WA.

Godunov, S. K. (1959). Finite difference methods for the computation of discontinuous solutions of the equations of fluid mechanics. *Math. Sbornik*, 47, 271-306.

Leon, A.S., Ghidaoui, M.S., Schmidt, A.R. and García, M.H. (2006). Godunov-type solutions for transient flows in sewers. *J. Hydraulic Engng.* 132(8), 800-813.

Leon, A.S., Ghidaoui, M.S., Schmidt, A.R. and García, M.H. (2007). *An efficient finite-volume scheme for modeling water hammer flows*. Contemporary Modeling of Urban Water Systems, Monograph 15, W. James (Editor in Chief).

Leon, A.S., Ghidaoui, M.S., Schmidt, A.R. and García, M.H. (2008). An efficient

second-order accurate shock capturing scheme for modeling one and two-phase water-hammer flows. *J. Hydraulic Engng.* 134(7), 970-983.

Leon, A.S., Ghidaoui, M.S., Schmidt, A.R. and García, M.H. (2009). Application of Godunov-type schemes to transient mixed flows. *J. Hydraulic Res.* 47(2), 147-156.

Leon, A.S., and Ghidaoui, M.S. (2010). “Discussion of numerical oscillations in pipe-filling bore predictions by shock-capturing models by Jose G. Vasconcelos, Steven J. Wright and Philip L. Roe.” *J. Hydraul. Engng.*, 136(6), 392393.

Leon, A.S., Liu, X., Ghidaoui, M.S., Schmidt, A.R. and García, M.H. (2010a). Junction and drop-shaft boundary conditions for modeling free-surface, pressurized, and mixed free-surface pressurized transient flows. *J. Hydraulic Engng.* 136(10), 705-715.

Leon, A.S., Ghidaoui, M.S., Schmidt, A.R. and García, M.H. (2010b). A robust two-equation model for transient mixed flows. *J. Hydraulic Res.* 48(1), 44-56.

LeVeque, R.J. (1998). Balancing source terms and flux gradients in high-resolution Godunov methods: the quasi-steady wave-propagation algorithm. *J. Comput. Phys.*, 146 (1), 346-365.

LeVeque, R.J. (2002). Finite volume methods for hyperbolic problems. Cambridge Press, Cambridge UK.

Sanders, B. F. (2001). High-resolution and non-oscillatory solution of the St. Venant equations in non-rectangular and non prismatic channels, *J. Hydraul. Research*, 39(3), 321-330.

Sanders, B. F. and Bradford, S. F. (2011). A network implementation of the two-component pressure approach for transient flow in storm sewers, *J. Hydraulic Engng.* 137(2), 158-172.

Song, C.C.S., Cardle, J.A., Leung, K.S. (1983). Transient mixed-flow models for storm sewers. *J. Hydraulic Engng.* 109(11), 1487-1503.

Toro, E. F. (2001). *Shock-capturing methods for free-surface shallow flows*, Wiley, LTD, Chichester, U.K.

Vasconcelos, J.G., Wright, S.J., Roe, P.L. (2006). Improved simulation of flow regime transition in sewers: Two-component pressure approach. *J. Hydraulic Engng.* 132(6), 553-562.

Yuan, M. (1984). Pressurized surges. MSc Thesis. Dept. of Civil and Mineral Engng., Univ. of Minnesota, Twin Cities MN.

Zhao, M., and Ghidaoui M. S. (2004). Godunov-type solutions for water hammer flows. *J. Hydraulic Engng.* 130(4), 341-348.

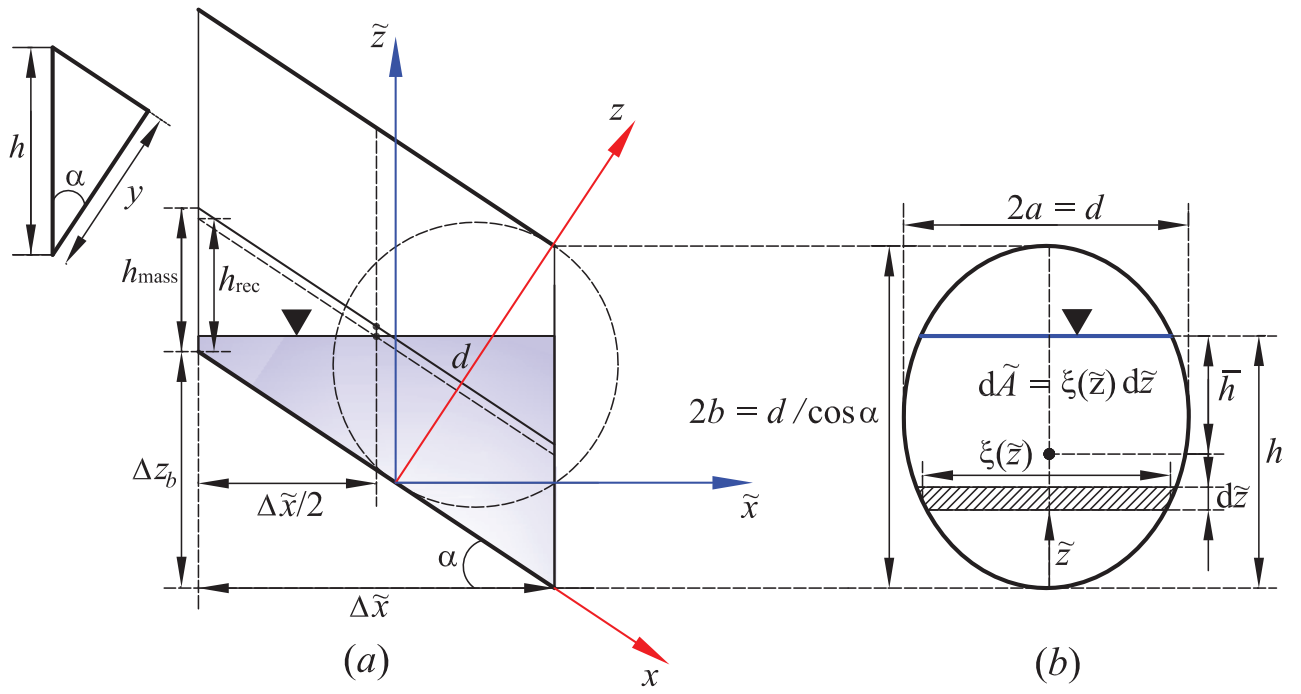


FIG. 1. Sketch of a sloped pipe

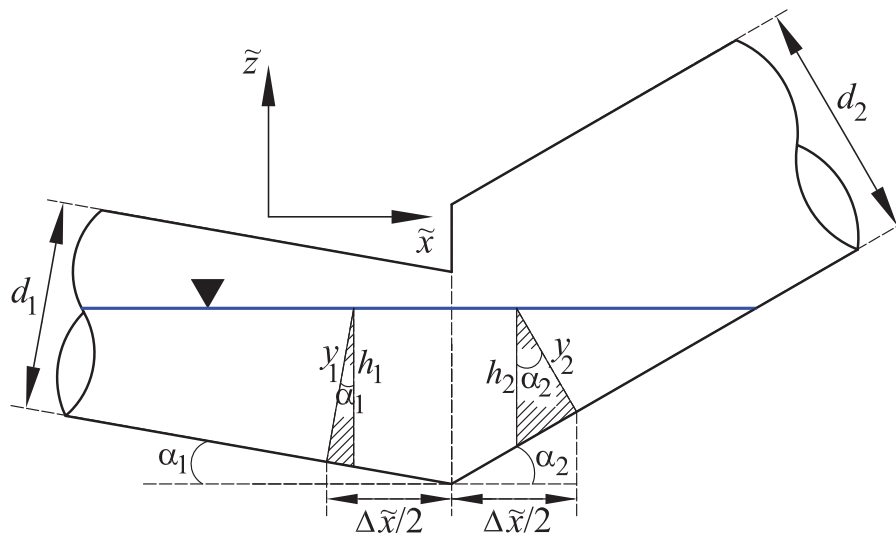


FIG. 2. Sketch of a two pipe system with different angles of inclination

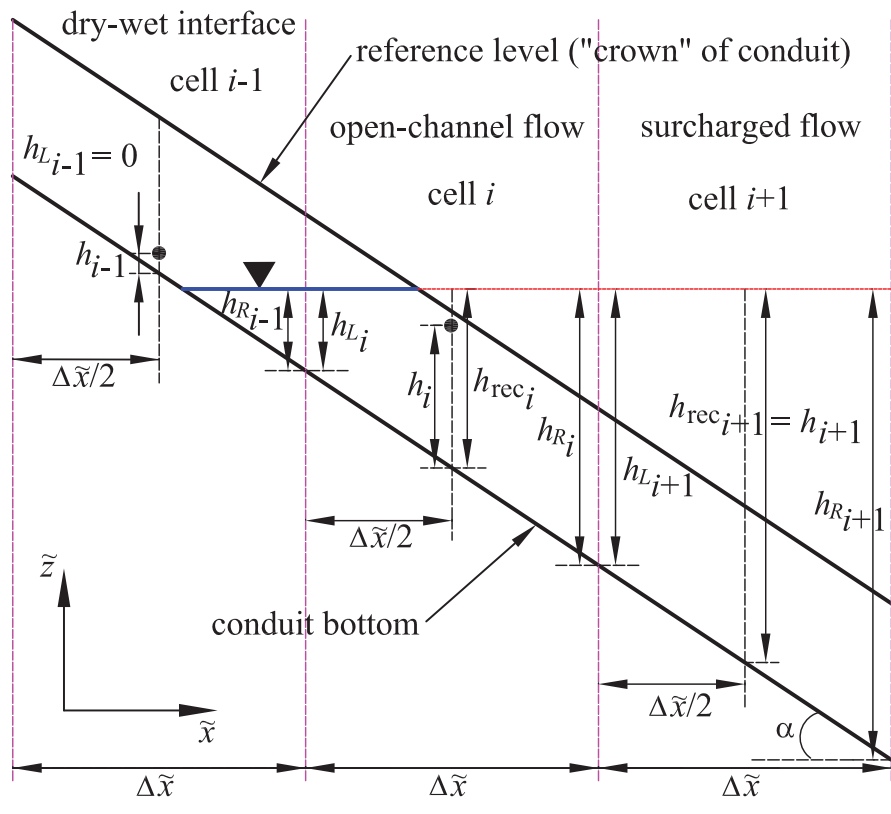


FIG. 3. Sketch that illustrates a dry-wet interface, open channel and surcharged flow conditions

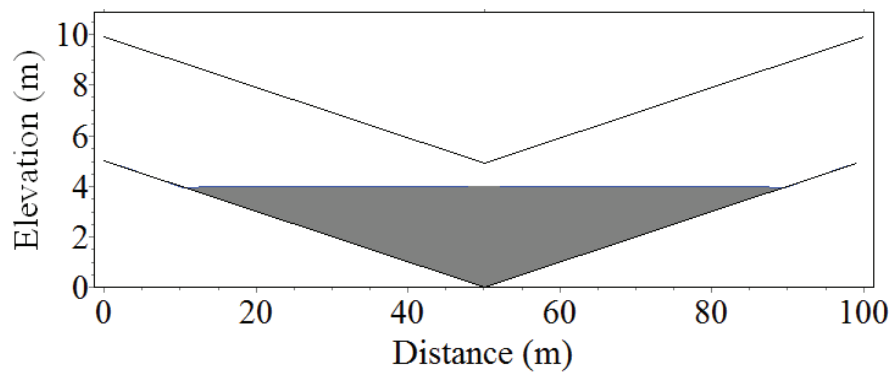


FIG. 4. Water surface profile for test 1 at time $t = 0$ s

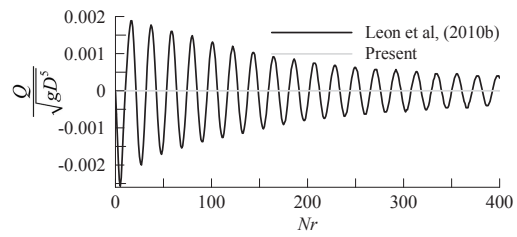


FIG. 5. Dimensionless flow discharge versus Nr for test 1 at midway of first conduit from left

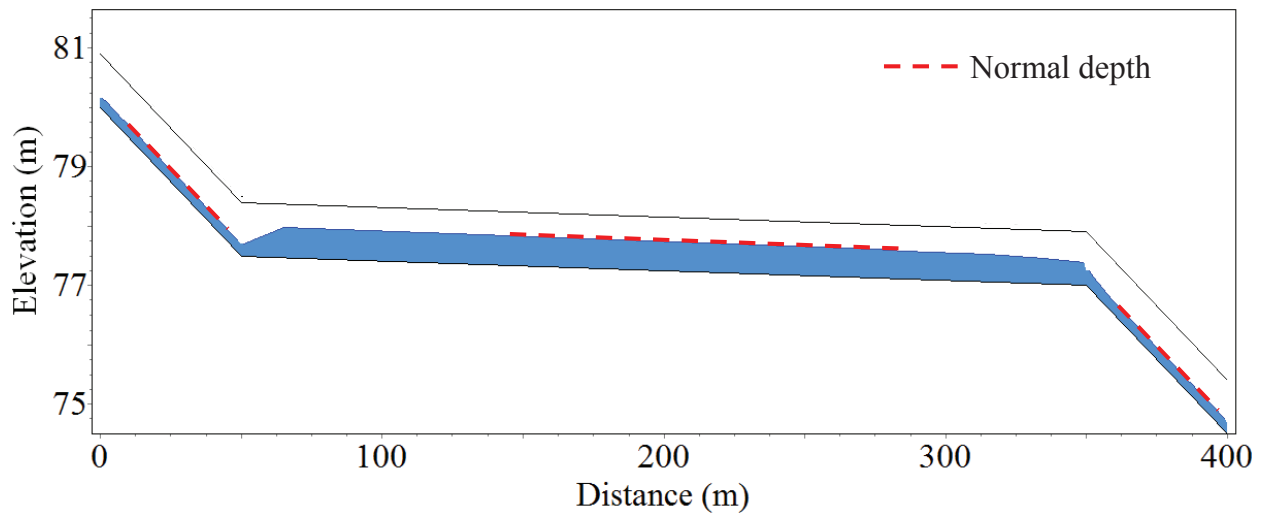


FIG. 6. Water surface profile for test 2 at time $t = 500$ s

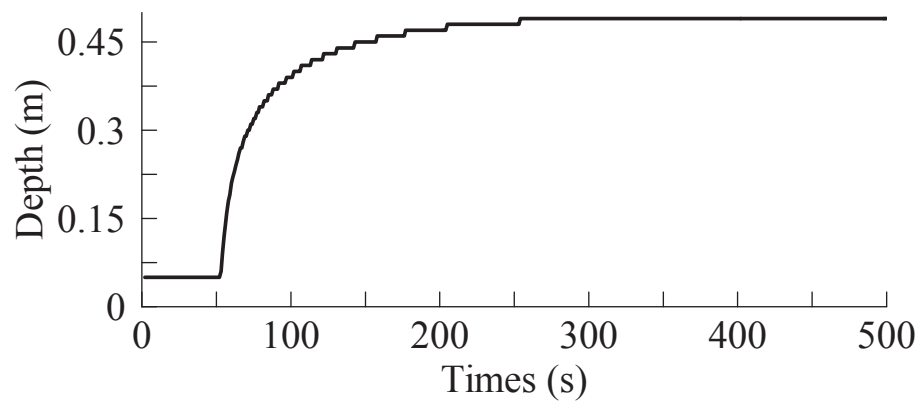


FIG. 7. Flow depth trace at midway of second conduit from left ($S_o=0.1667\%$)

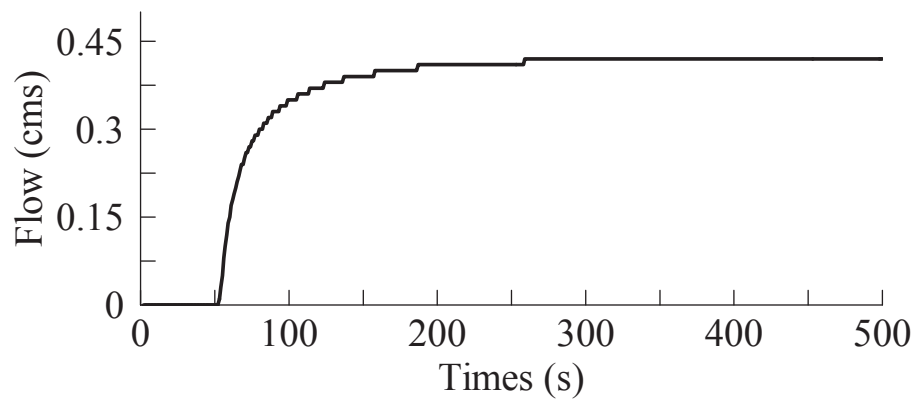


FIG. 8. Flow discharge trace at midway of second conduit from left ($S_o = 0.1667\%$)

$t = 0.1\text{s}$

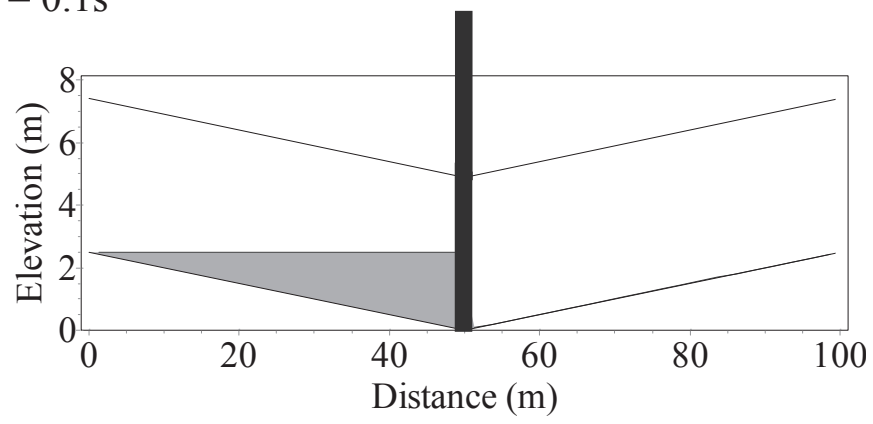


FIG. 9. Water surface profile for test 3 at time $t = 0.1\text{ s}$

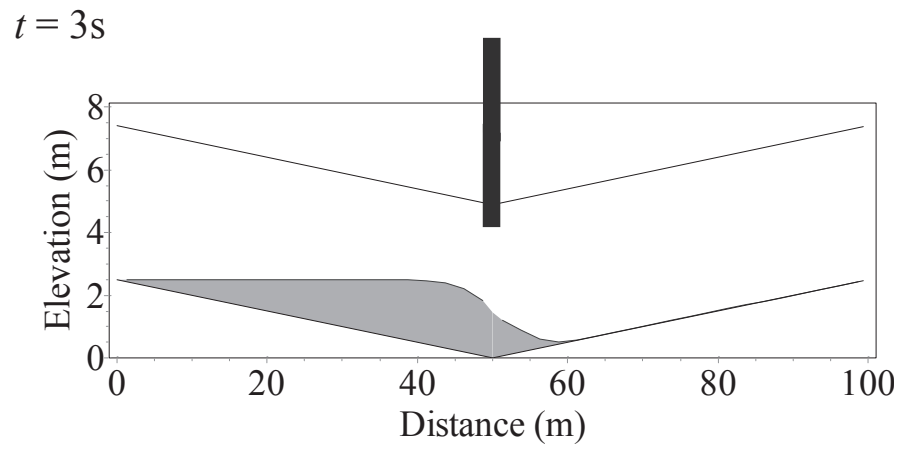


FIG. 10. Water surface profile for test 3 at time $t = 3\text{ s}$

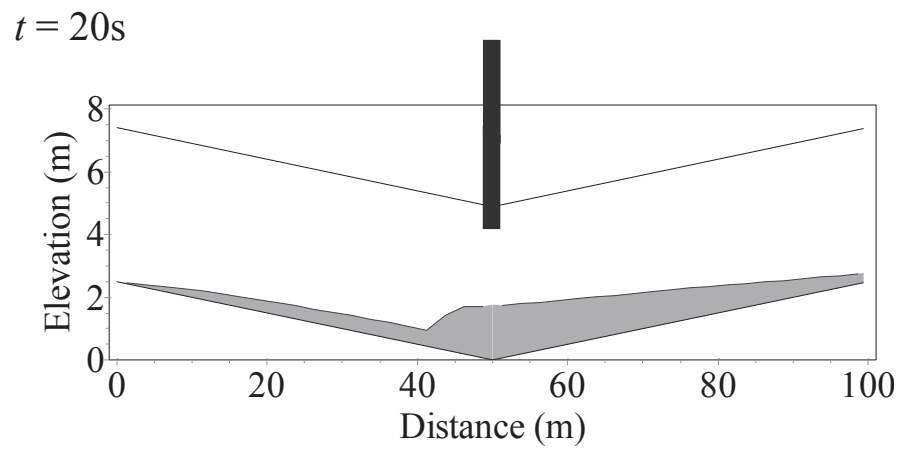


FIG. 11. Water surface profile for test 3 at time $t = 20\text{ s}$

$t = 240\text{s}$

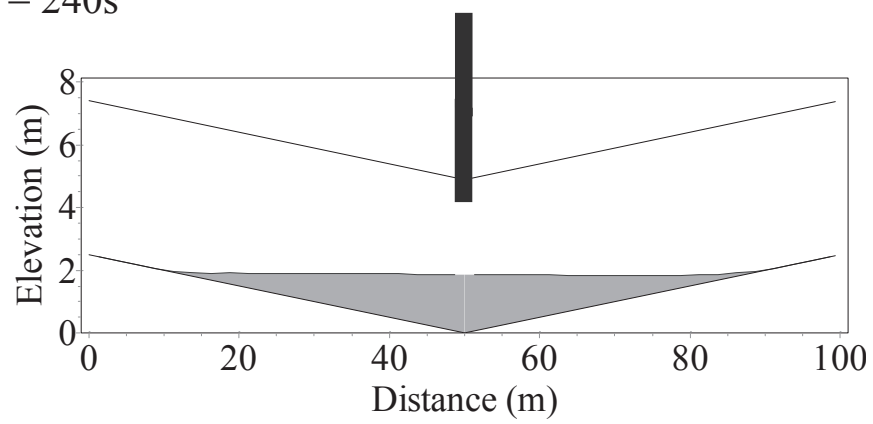


FIG. 12. Water surface profile for test 3 at time $t = 240\text{ s}$

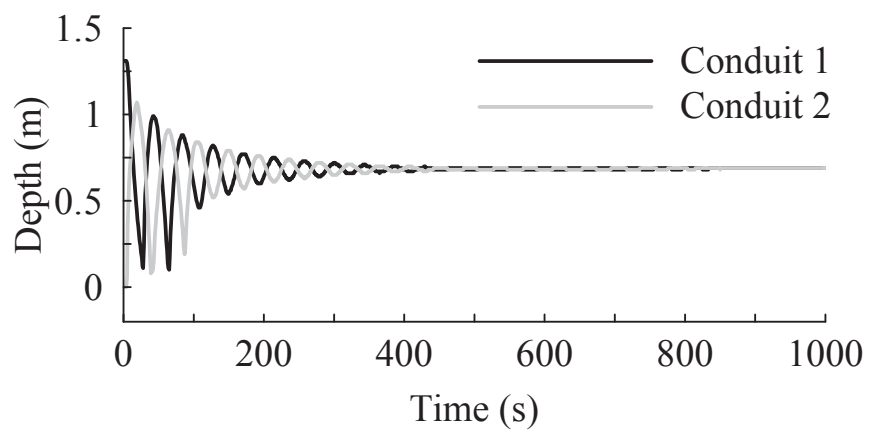


FIG. 13. Piezometric depth trace at midway of conduits 1 and 2 for test 3

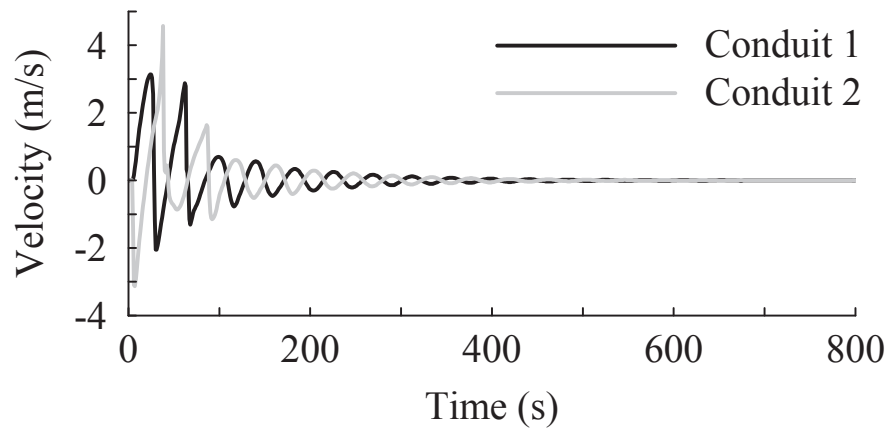


FIG. 14. Flow velocity trace at midway of conduits 1 and 2 for test 3

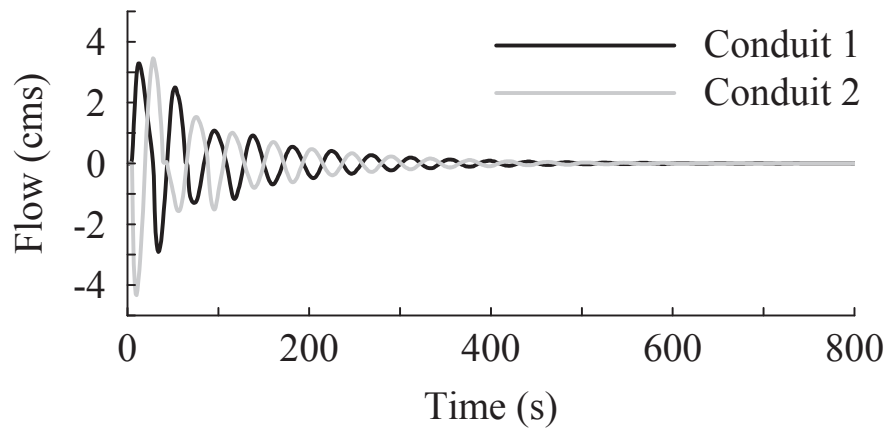


FIG. 15. Flow discharge trace at midway of conduits 1 and 2 for test 3

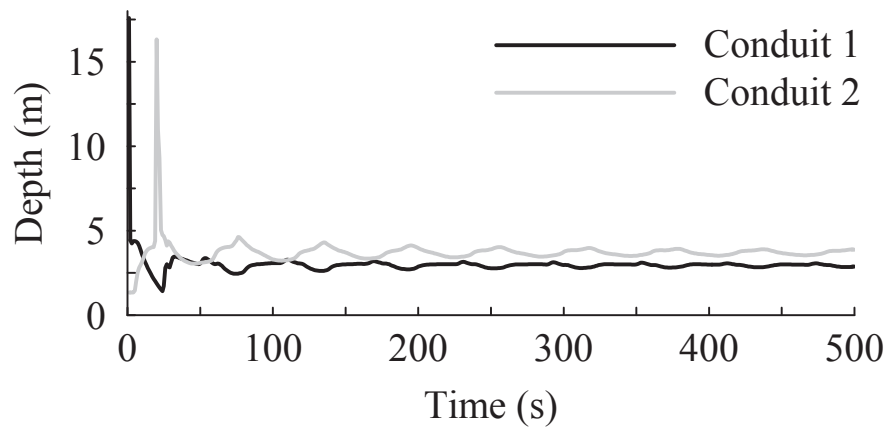


FIG. 16. Piezometric depth trace at midway of conduits 1 and 2 for test 4

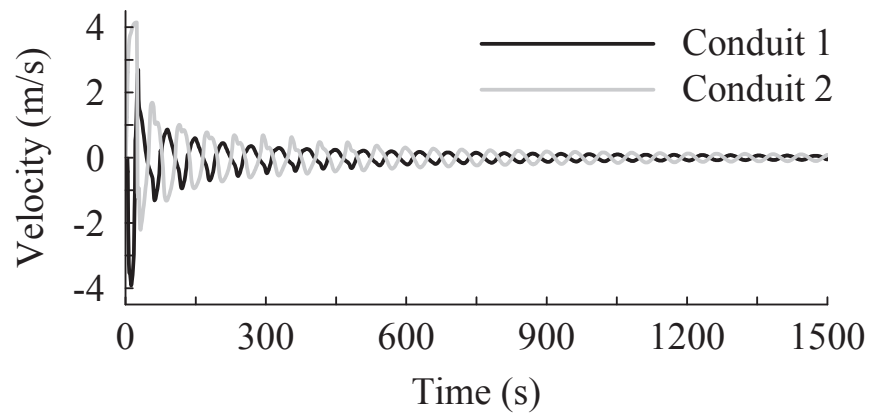


FIG. 17. Flow velocity trace at midway of conduits 1 and 2 for test 4

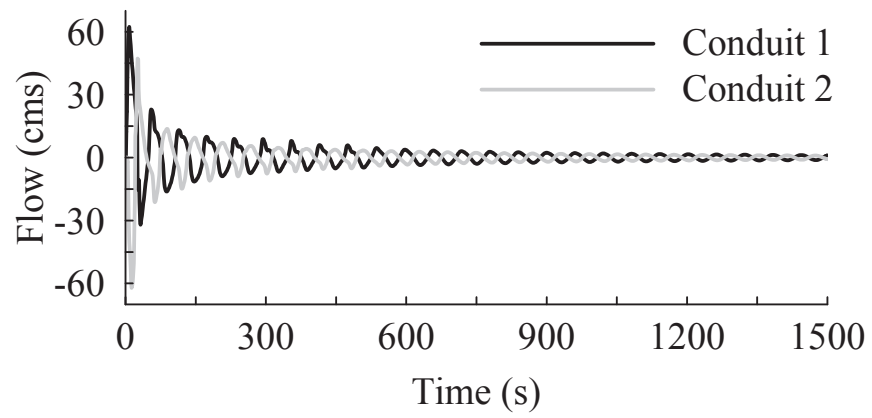


FIG. 18. Flow discharge trace at midway of conduits 1 and 2 for test 4

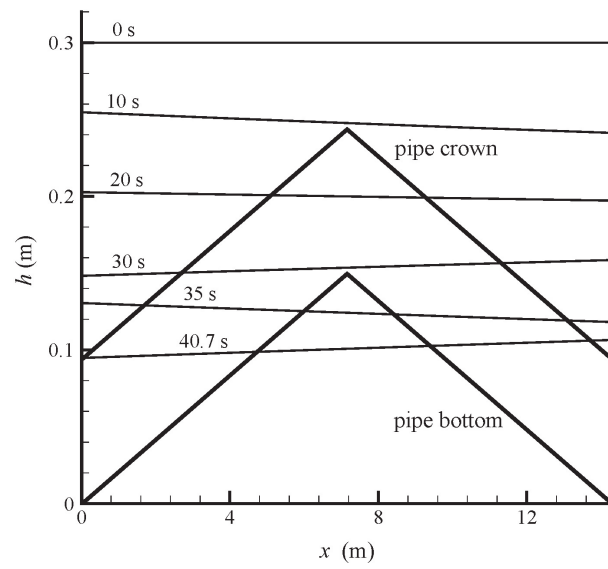


FIG. 19. Simulated piezometric depth snapshots

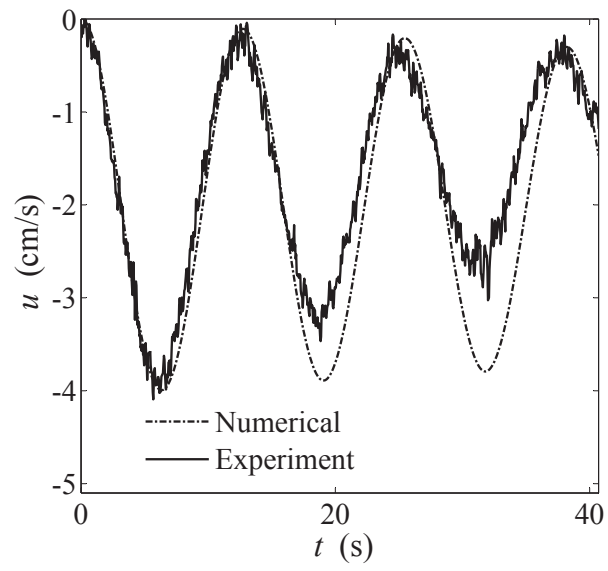


FIG. 20. Measured and computed velocities at 9.9 m from the upstream end for the experiments of Vasconcelos et al. (2006)

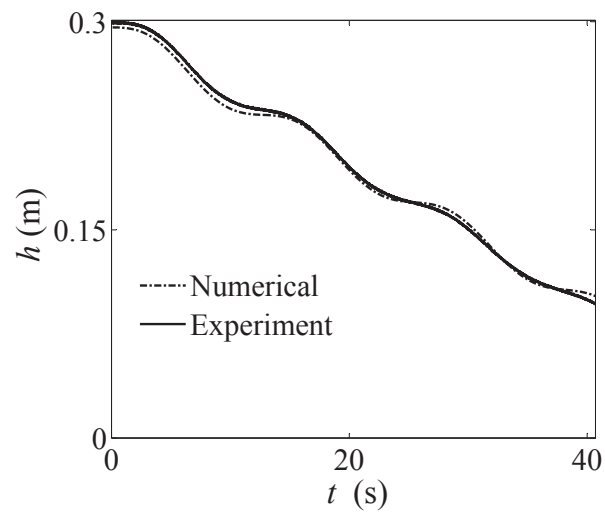


FIG. 21. Measured and computed piezometric depths at 14.1 m from the upstream end for the experiments of Vasconcelos et al. (2006)

TABLE 1. Maximum discharge and maximum water depth fluctuation (with respect to initial conditions) attained at the end of various time steps

Description	Time steps		
	10^3	10^5	10^7
Flow discharge (m^3/s)	$O(10^{-5})$	$O(10^{-5})$	$O(10^{-5})$
Water depth fluctuation (m)	$O(10^{-8})$	$O(10^{-8})$	$O(10^{-8})$